Electronic Supplementary Information

Plasmon photothermal-promoted solar photocatalytic hydrogen production over $CoCr_2O_4$/g-C_3N_4 heterojunction

Renzhi Xiong, Changcun Tang, Kunjiao Li, Jiabao Wan, Weifeng Jia, Yanhe Xiao,

Baochang Cheng and Shuijin Lei*

School of Physics and Materials Science, Nanchang University, Nanchang, Jiangxi 330031,

P. R. China

*To whom correspondence should be addressed. E-mail: shjlei@ncu.edu.cn

Supplementary Figures

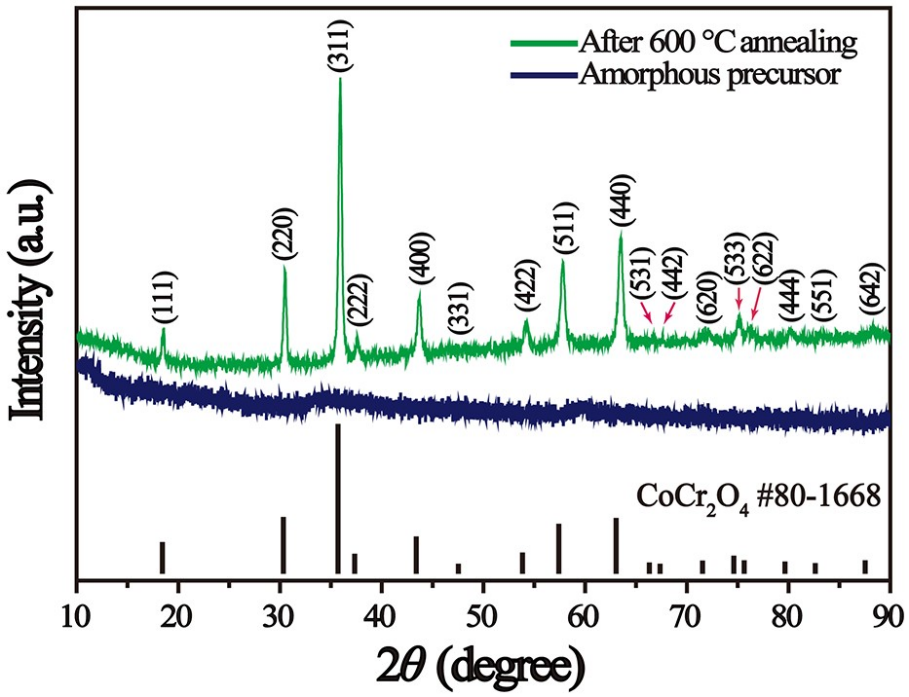

Fig. S1 XRD patterns of the $CoCr_2O_4$ sample before and after annealing.

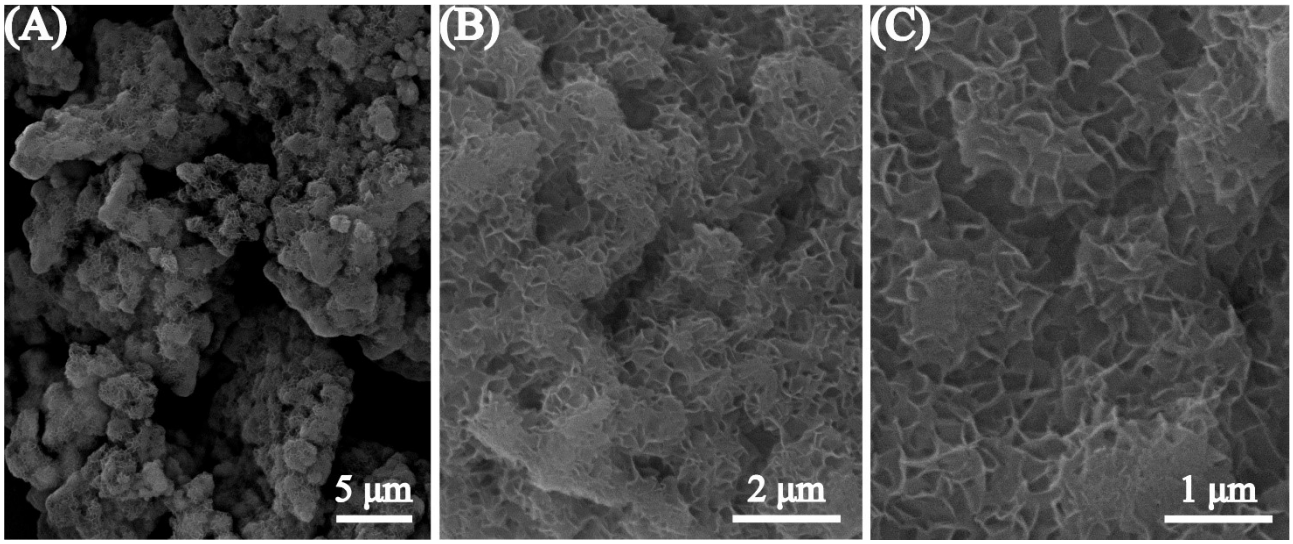

Fig. S2 SEM images of the amorphous $CoCr_2O_4$ precursor.

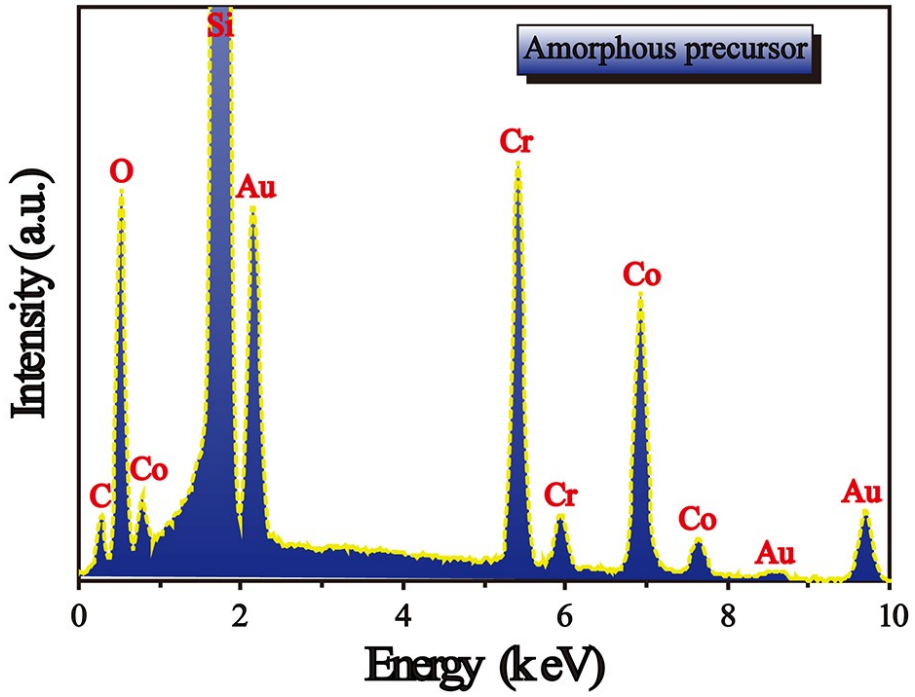

Fig. S3 EDS spectrum of the amorphous $CoCr_2O_4$ precursor.

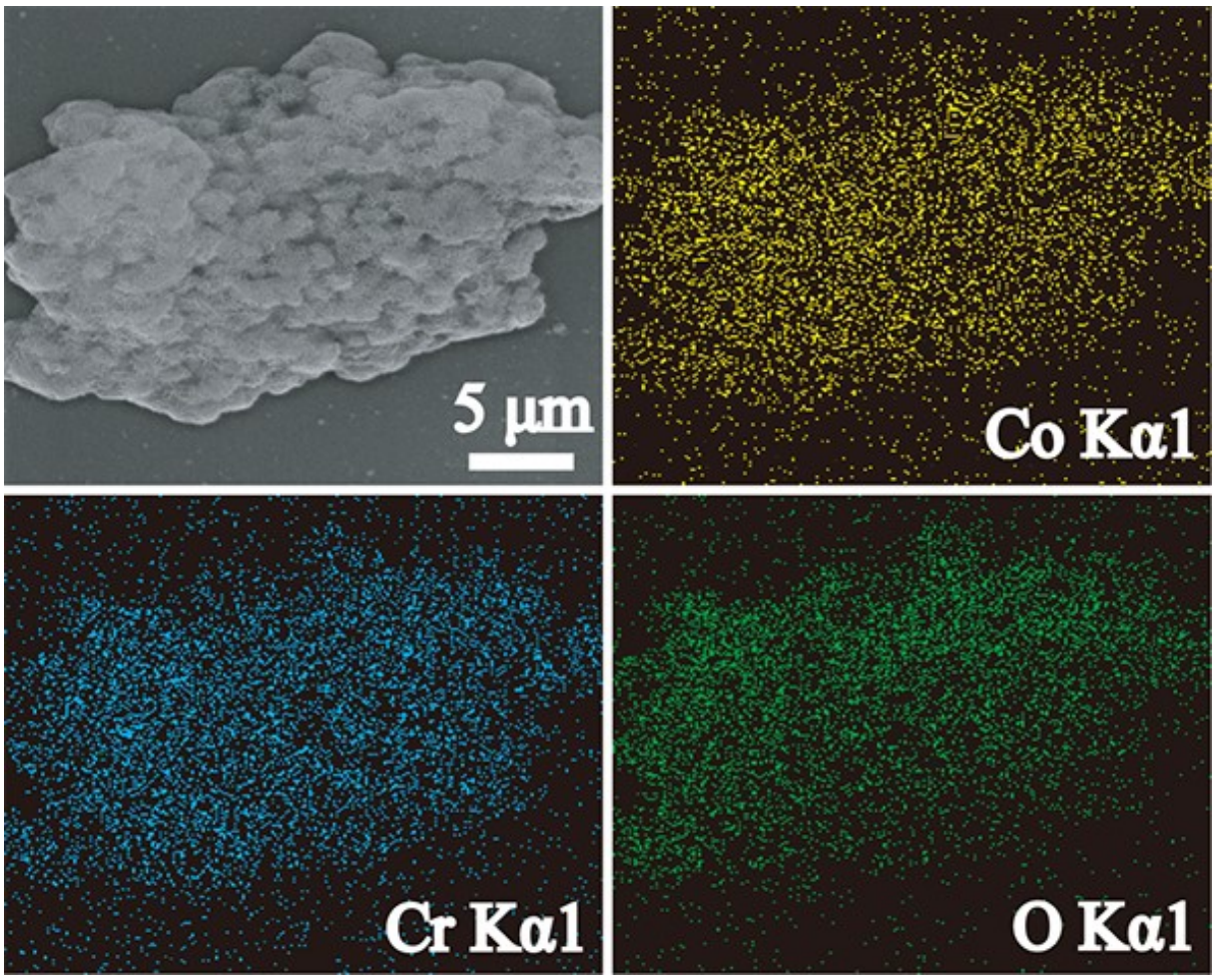

Fig. S4 EDS elemental mapping images of the amorphous $CoCr_2O_4$ precursor.

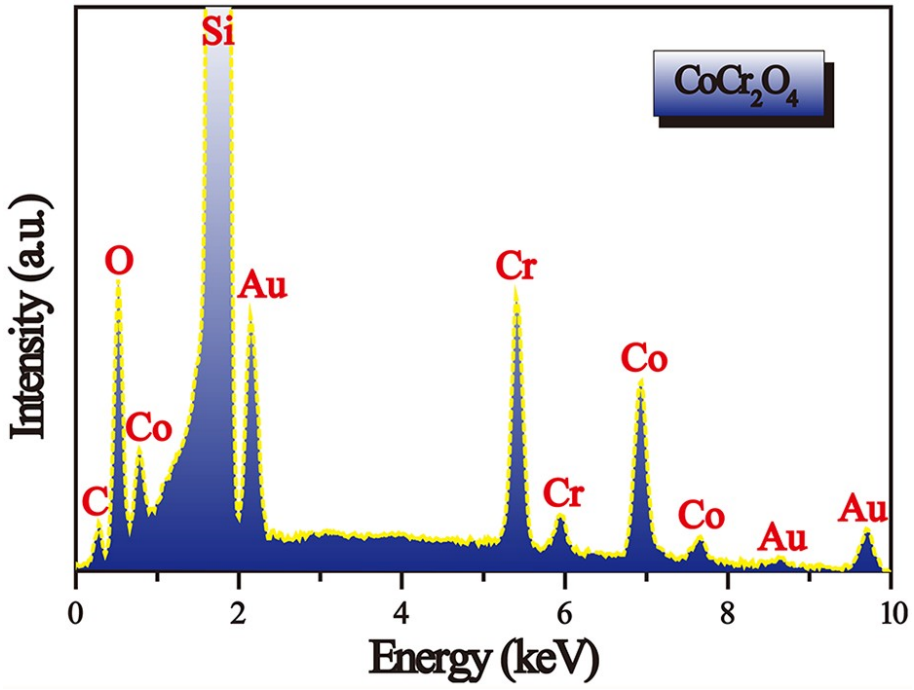

Fig. S5 EDS spectrum of the $CoCr_2O_4$ sample after annealing at 600 °C.

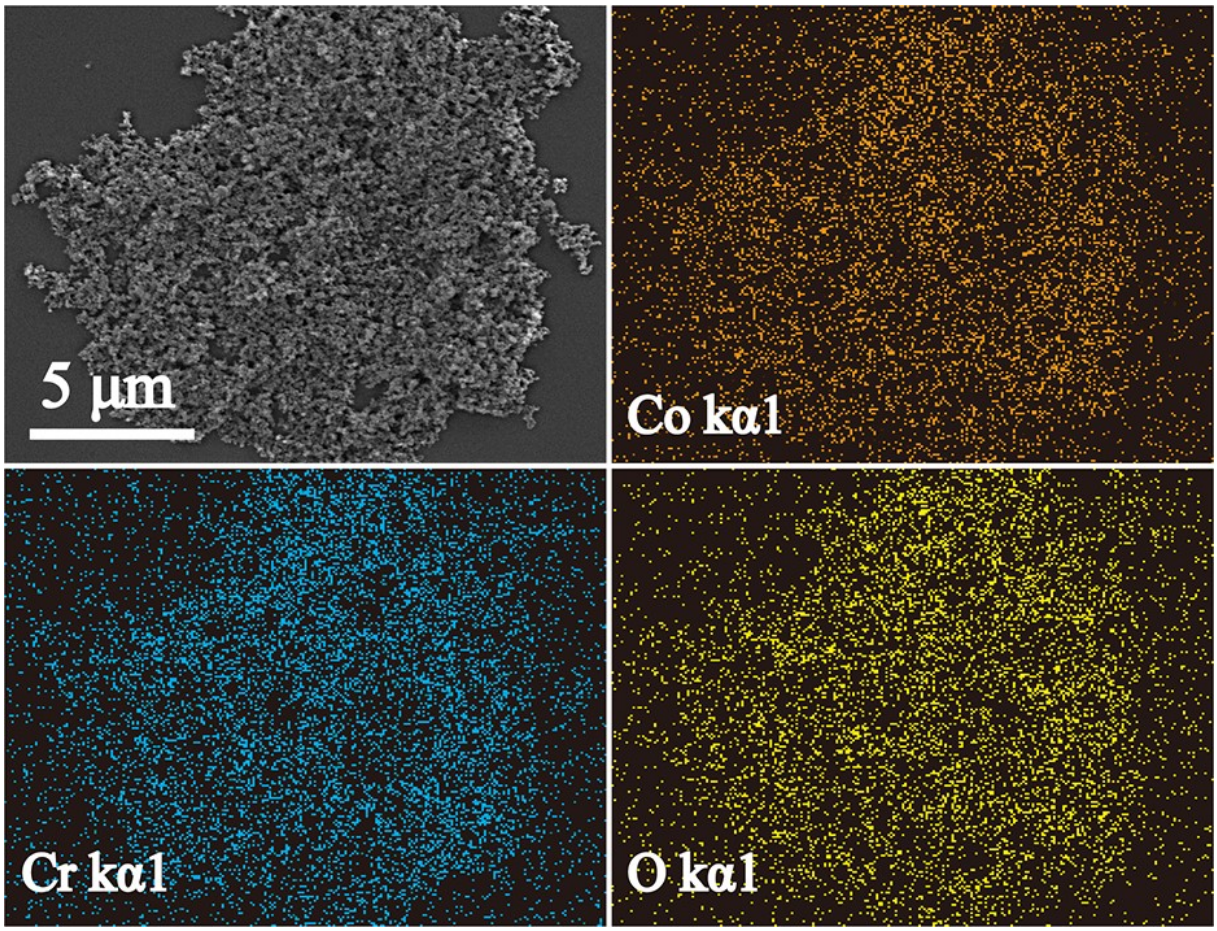

Fig. S6 EDS elemental mapping images of the $CoCr_2O_4$ sample after annealing at 600 °C.

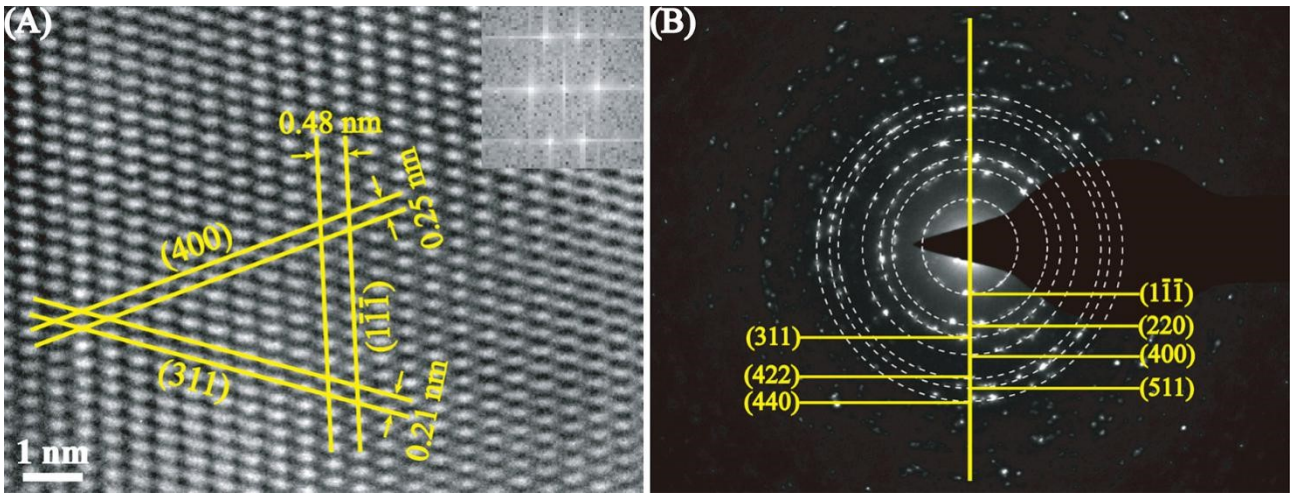

Fig. S7 (A) HRTEM image (inset: the corresponding FFT patterns) and (B) SAED patterns of the $CoCr_2O_4$ sample after annealing at 600 °C.

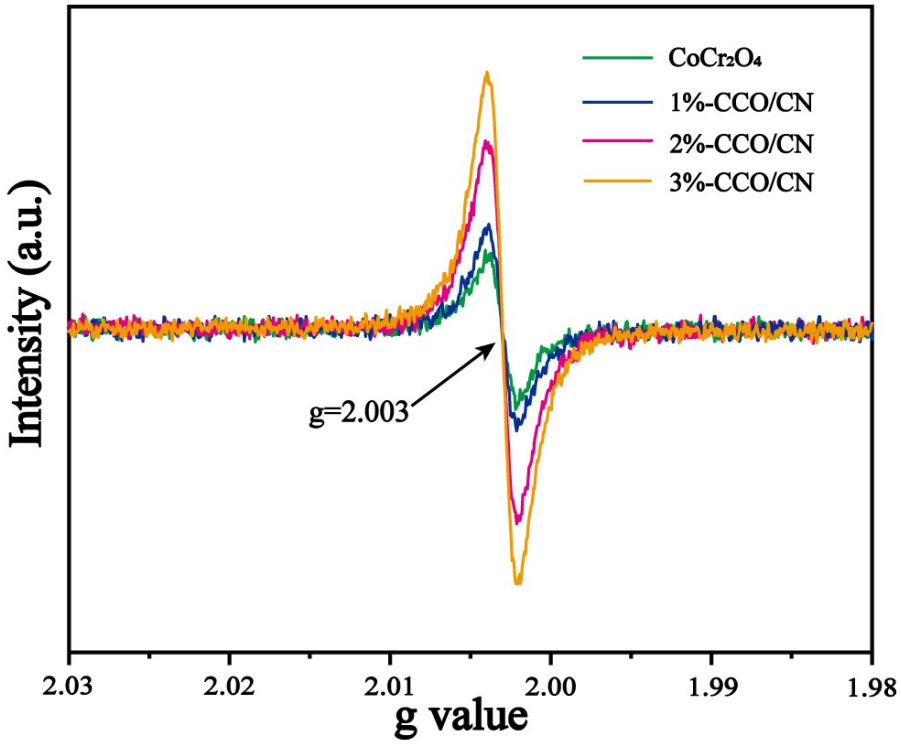

Fig. S8 EPR spectra of the $CoCr_2O_4$, 1%-CCO/CN, 2%-CCO/CN, and 3%-CCO/CN samples.

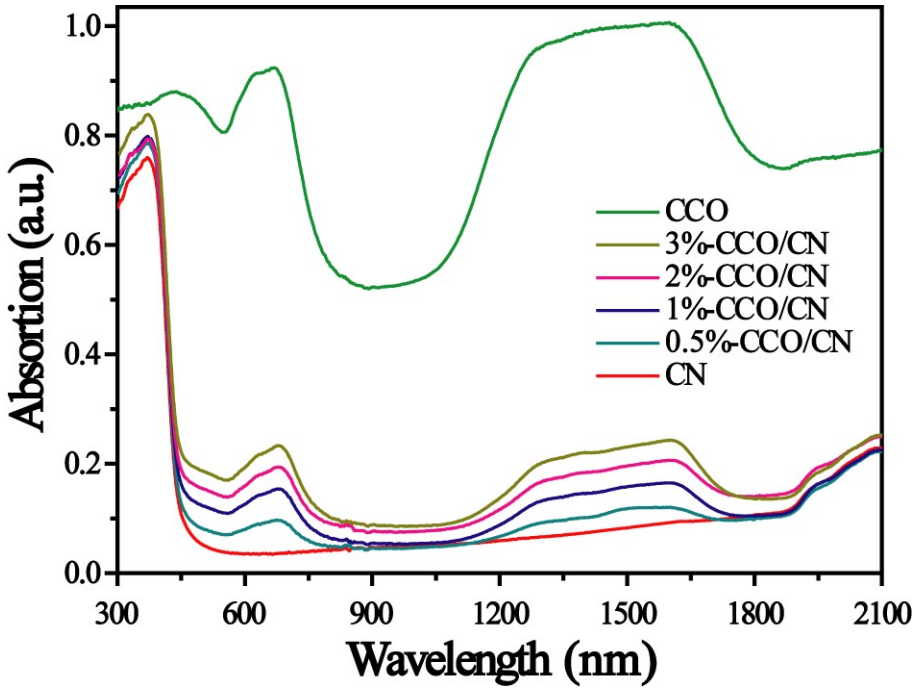

Fig. S9 The full spectra of UV-Vis-NIR absorption of all the fabricated samples.

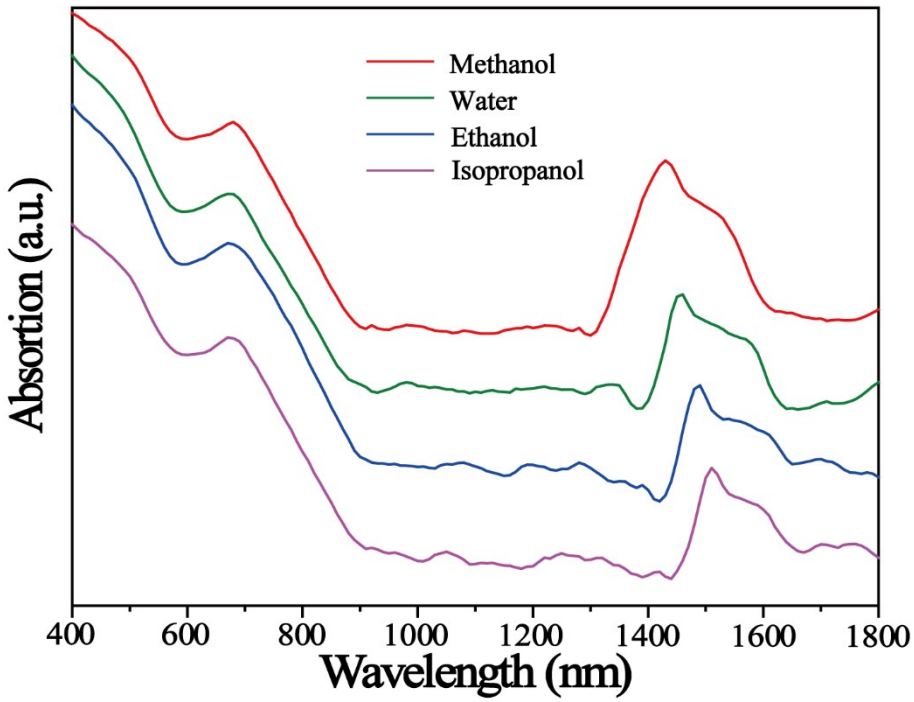

Fig. S10 Solution-phase UV-Vis-NIR absorption spectra of the prepared $CoCr_2O_4$ nanoparticles dispersed in diverse solvents with different refractive indices.

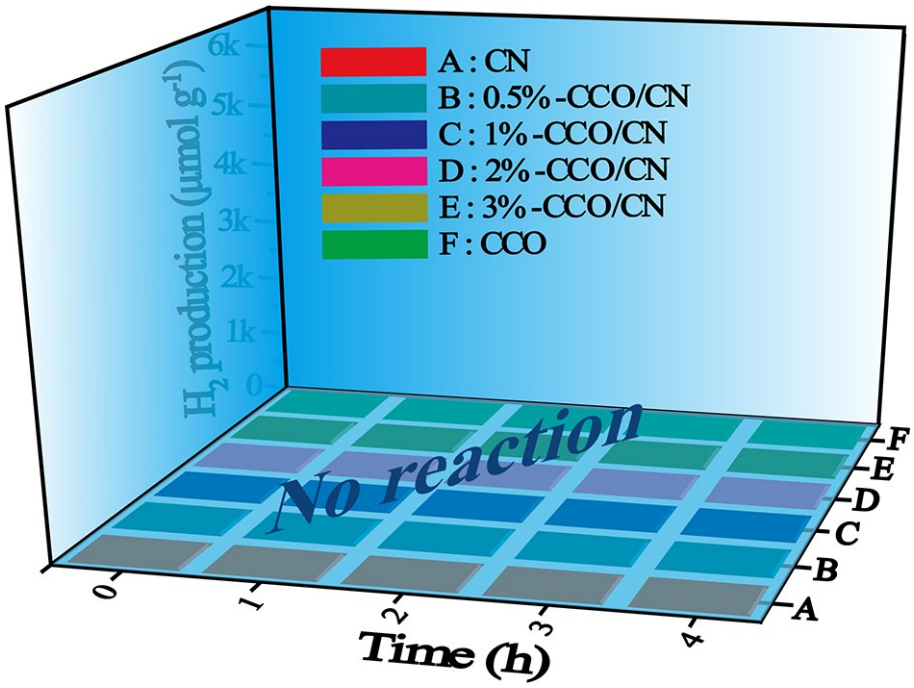

Fig. S11 The photocatalytic hydrogen production activity of all the fabricated samples under IR illumination.

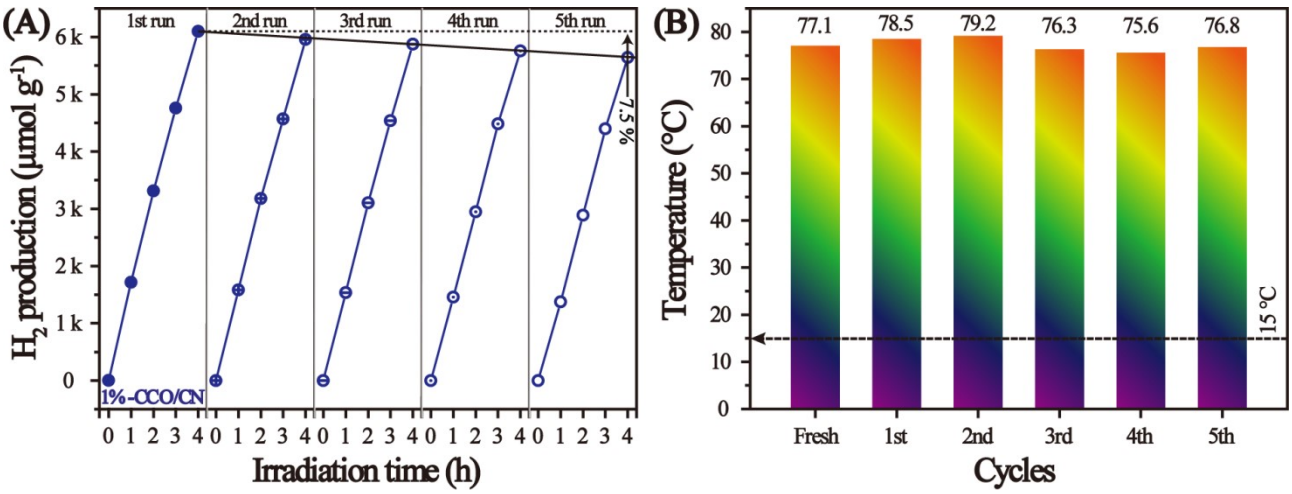

Fig. S12 (A) Cycling runs for the photocatalytic hydrogen production in presence of the 1%-CCO/CN photocatalyst and (B) the corresponding photothermal induced surface temperature of the recycled 1%-CCO/CN photocatalyst after each cycle.

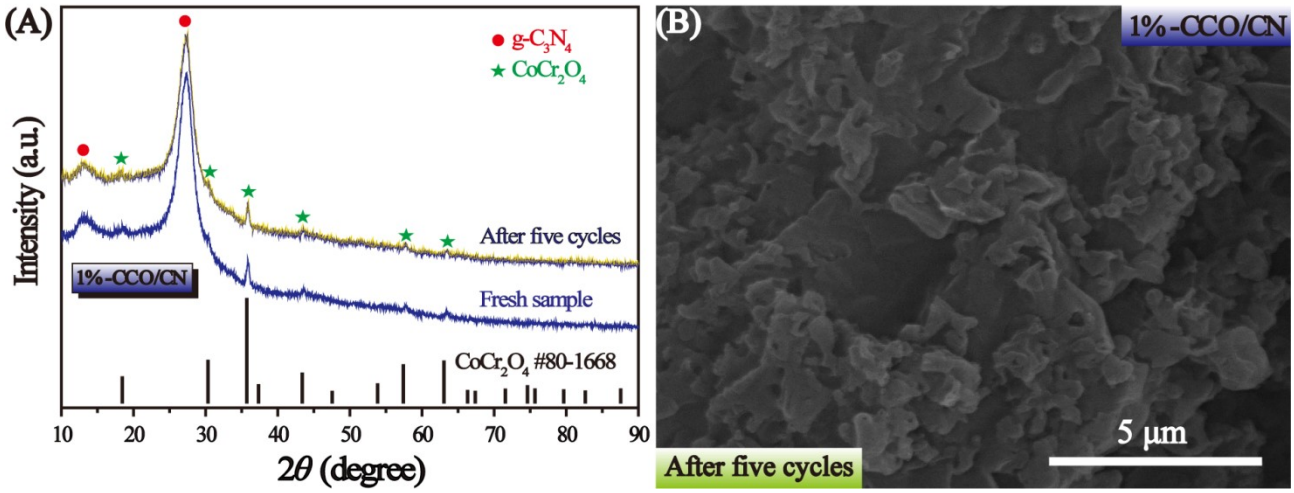

Fig. S13 (A) XRD patterns of 1%-CCO/CN before and after five runs of photocatalytic hydrogen production, and (B) SEM image of 1%-CCO/CN after five cycles of photocatalytic hydrogen production.

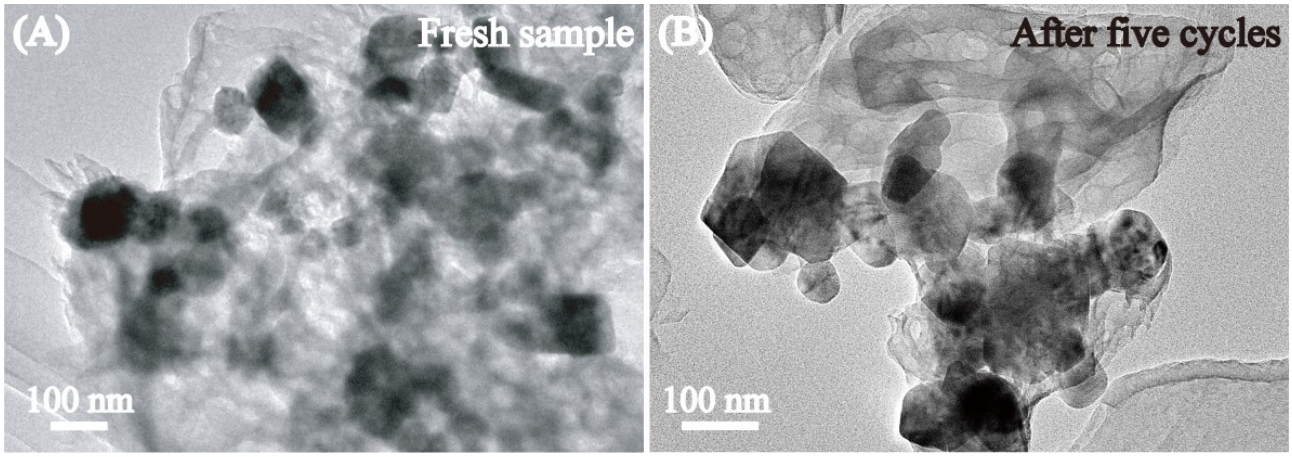

Fig. S14 TEM images of the 1%-CCO/CN sample (A) before photocatalytic reactions, and (B) after five runs of photocatalytic hydrogen production.

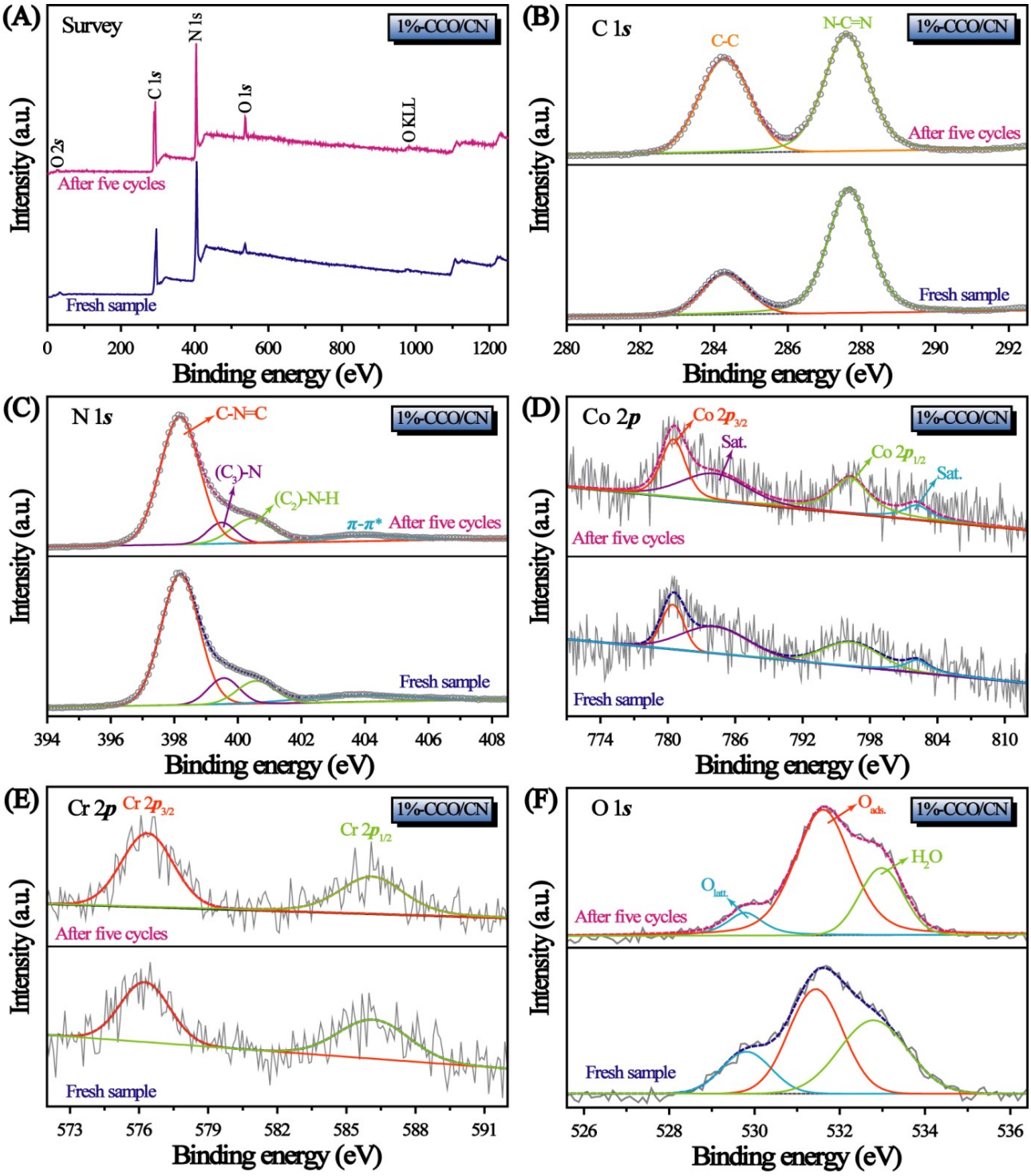

Fig. S15 XPS spectra of the 1%-CCO/CN sample before and after five runs of photocatalytic hydrogen production: (A) survey spectra, and the core-level spectra of (B) C 1s, (C) N 1s, (D) Co 2p, (E) Cr 2p, and (F) O 1s.

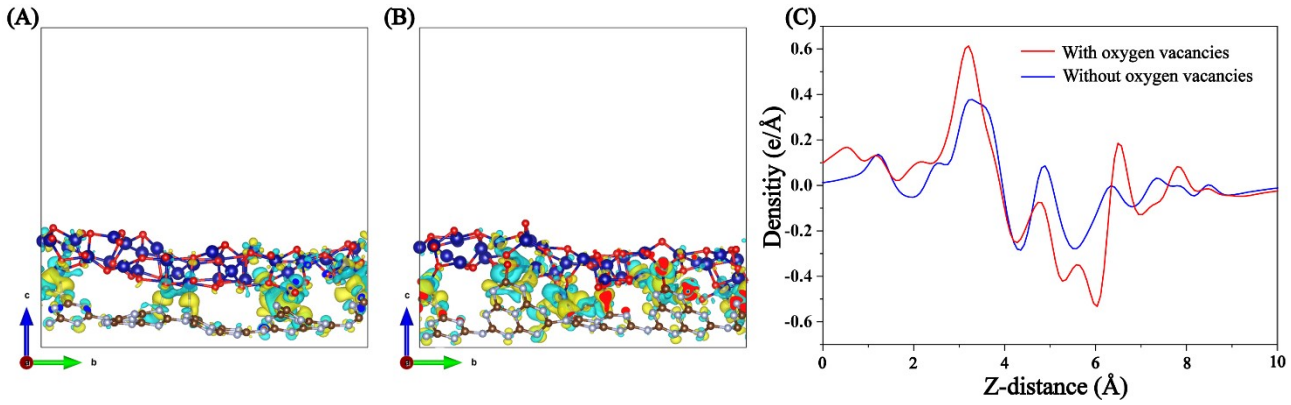

Fig. S16 The charge density difference for the $CoCr_2O_4$/g-C_3N_4 heterostructures (A) without oxygen vacancies and (b) with few oxygen vacancies. The cyan and yellow areas represent electron depletion and accumulation, respectively. (C) Planar-averaged electron density along the Z direction for the $CoCr_2O_4$/g-C_3N_4 heterostructures without and with oxygen vacancies.